

# NUMERICAL STUDY ON ACOUSTIC RECEPTIVITY OF COMPRESSIBLE LAMINAR FLOW OVER A FLAT PLATE WITH MODIFIED SUPER-ELLIPSE LEADING EDGE

Binzhuo Xu & Zhenli Chen\*

School of Aeronautics, Northwestern Polytechnical University, Xi'an 710072, China National Key Laboratory of Aircraft Configuration Design, Xi'an 710072, China

#### **Abstract**

Receptivity determines the initial amplitude and phase of unstable waves in the boundary layer, which affect the transition process. It is necessary to understand the process of how external freestream disturbances enter the boundary layer and are transformed to unstable waves. In this work, the acoustic receptivity of compressible laminar flow past a flat plate with super-ellipse leading-edge were studied using numerical method, which is based on the linearized compressible Navier-Stokes (N-S) equations. In the steady, base flow, a plane acoustic wave disturbance at specific frequency is enforced to obtain the response of acoustic disturbance in the boundary layer, and the unstable Tollmien-Schlichting (T-S) wave is excited. The effects of leading-edge aspect ratio, Mach number and disturbance frequency on receptivity and stability are studied. The wavelength conversion mechanism of subsonic boundary-layer receptivity is confirmed, and it is found that Mach number and disturbance frequency have strong effects on eigenfunction of T-S wave, however, the leading-edge aspect ratio has almost no effect. The receptivity coefficient increases with the decrease of the leading-edge aspect ratio, but with increase of Mach number and disturbance frequency. As Mach number and disturbance frequency increase, the low branch unstable location goes upstream. Local adverse pressure gradient caused by different leading-edge aspect-ratio has an important impact on the receptivity process, and the receptivity coefficient increases with the increase of the local adverse pressure gradient. The locations of pressure-gradient peak and onset of zero-pressure gradient move downstream with increasing leading-edge aspect ratio, but the sub-critical Mach number has very weak effect.

**Keywords:** leading-edge acoustic receptivity, compressible, boundary layer, Tollmien-Schlichting wave, wavelength conversion

#### 1. Introduction

Disturbances in the freestream, such as sound or vorticity, enter the boundary layer as steady or unsteady disturbances of the basic flow. This process is called receptivity by Morkovin[1], and it establishes the initial conditions of disturbance amplitude, frequency, and phase for the stability analysis of laminar flow.

Generally, the boundary-layer transition process can be divided into five stages: receptivity, linear growth, nonlinear interaction, secondary instability and breakdown[2]. Receptivity concerns the generation of instability waves in the boundary layer, rather than their evolution. For incompressible flows, receptivity has many different paths which introduce a disturbance into the boundary layer. These include the interaction of freestream sound or turbulence with leading-edge surface curvature discontinuities, or surface inhomogeneities[3]. Since the boundary layer is enforced by freestream disturbances, the equations or boundary conditions are no longer homogeneous, and the receptivity is no longer an eigenvalue problem, but an initial-value problem. Thus, the governing equation of receptivity is usually Navier-Stokes (N-S) equations with appropriate boundary conditions and initial

conditions. The disturbances in laminar boundary layer are of great importance on stability and transition prediction, so it is necessary to understand how the freestream disturbances enter the boundary layer and transform into unstable waves, i.e., to solve the receptivity problem.

For receptivity in the leading-edge region, the Reynolds number is assumed to be large so that the flow can be divided into two regions of the outer flow and inner flow in the boundary layer, the outer flow corresponds to an inviscid interaction of the small-amplitude freestream disturbance with the body. This inviscid interaction provides the distributions of pressure and velocity that drive the unsteady motion in the boundary layer. Near the leading edge, the motion satisfies the linearized, unsteady, boundary-layer equation (LUBLE) for two-dimensional base flow[3]. The LUBLE contains  $u'U_x$  and  $V'u_y$ , which do not appear in the Orr-Sommerfeld equation (OSE) and are nonparallel meanflow effects that occur on the short-scale of the unsteady disturbance. Further downstream from the leading edge, a consistent approximation leads to the classical large-Reynolds-number, small wavenumber approximation to the OSE. Goldstein examined the asymptotic matching of these two regions, and showed that the first Lam-Rott asymptotic eigenfunction of the LUBLE, with coefficient  $C_1$ , matches onto the T-S wave that becomes unstable farther downstream in the OSE region[5]. Hence, the amplitude of the T-S wave is linearly proportional to  $C_1$ , which we call the theoretical leading-edge receptivity coefficient[4]. The crucial role of short-scale streamwise variations of the mean flow in natural receptivity processes was first elucidated by Goldstein, utilizing high-Reynoldsnumber asymptotic analysis[4, 5]. He showed that natural receptivity occurs in regions where the mean flow changes rapidly in the streamwise direction, invalidating the parallel-flow assumption of the OSE. The regions where natural receptivity occurs can be separated into two classes. The first class consists of body leading-edge regions, where the boundary layer is thin and growing rapidly[4]. The second class contains regions farther downstream in the boundary layer, where some local feature causes the mean flow to adjust on a short streamwise length scale[5].

Acoustic receptivity can be expressed either in terms of (a) a leading-edge receptivity coefficient defined as the ratio of the T-S amplitude in the leading-edge region to the amplitude of the freestream acoustic disturbances

$$K_{LE} = |u'_{TS}|_{LE} / |u'_{ac}|_{fs} \tag{1}$$

or (b) a Branch-I receptivity coefficient defined as the T-S amplitude at Branch-I normalized with the amplitude of the freestream acoustic disturbances

$$K_I = \left| u'_{TS} \right|_I / \left| u'_{ac} \right|_{LE} \tag{2}$$

where "| " denotes absolute value or root-mean-square (rms). Haddad & Corke argued that the appropriate receptivity coefficient is  $K_{LE}$  because it is based strictly on local properties of the leading-edge region, where  $K_I$  depends on the pressure gradient history from the leading edge to Branch-I[5]. Moreover, because of pressure gradients,  $K_{LE}$  decreases with nose radius and  $K_I$  increases with nose radius, which could lead to some confusion. These arguments are compelling, but utilitarian issues sometimes argue for the use of  $K_I$ . For example, it is impossible for an experiment to measure  $|u'_{TS}|_{LE}$ ; most transition correlation schemes begin with Branch-I calculations; the pressure gradient history can easily be accounted for by OSE calculations up to a region near the leading edge[3].

### 2. Simulation Method

# 2.1 Governing Equations

To study the acoustic receptivity of compressible laminar flow, the compressible Navier-Stokes (N-S) equations suitable for the receptivity simulation are adopted. The dimensional N-S equations are nondimensionalized by the freestream values. Then the flow variables are decomposed into a base and a perturbation components, which can be written as

$$U = \bar{U} + U' \tag{3}$$

where can be  $\rho$ ,  $u_i$ , p, etc., the bar means the base-flow variable, and the prime means the linear disturbance.

Applying this decomposition and dropping the nonlinear terms in disturbances, the steady baseflow equations are obtained

$$(\bar{\rho}\,\bar{u}_i)_i = 0 \tag{4}$$

$$\bar{\rho} \, \bar{u}_{j} \bar{u}_{i,j} = -\bar{p}_{,i} + \frac{1}{\text{Re}} [(\bar{\lambda} \, \bar{u}_{j,j})_{,i} + (2\bar{\mu} \, \bar{S}_{ij})_{,j}]$$
(5)

$$\bar{\rho}\,\bar{u}_{j}\bar{T}_{,j} + (\gamma - 1)\bar{\rho}\,\bar{T}\,\bar{u}_{j,j} = \frac{\gamma}{\Pr \operatorname{Re}} [\bar{\kappa}\,\bar{T}_{,i}]_{,i} + \frac{\gamma(\gamma - 1)M^{2}}{\operatorname{Re}} [\bar{\lambda}\,\bar{S}_{ii}\bar{S}_{jj} + 2\bar{\mu}\,\bar{S}_{ij}\bar{S}_{ij}]$$
(6)

$$\bar{p} = \frac{\bar{\rho}\,\bar{T}}{\gamma M^2} \tag{7}$$

and the unsteady linearized perturbation equations are obtained

$$\rho'_{,t} + (\bar{\rho} \, u'_{i})_{,i} + (\rho' \bar{u}_{i})_{,i} = 0 \tag{8}$$

$$\bar{\rho} u'_{i,t} + \bar{\rho} \bar{u}_{j} u'_{i,j} + \bar{\rho} u'_{j} \bar{u}_{i,j} + \rho' \bar{u}_{j} \bar{u}_{i,j} = -p'_{,i} + \frac{1}{\text{Re}} [(\bar{\lambda} u'_{j,j})_{,i} + (\lambda' \bar{u}_{j,j})_{,i} + (2\bar{\mu} S'_{ij})_{,j} + (2\mu' \bar{S}_{ij})_{,j}]$$
(9)

$$\bar{\rho} T'_{,t} + \bar{\rho} \bar{u}_{j} T'_{,j} + \bar{\rho} u'_{j} \bar{T}_{,j} + \rho' \bar{u}_{j} \bar{T}_{,j} =$$

$$(1 - \gamma) [\rho' \bar{T} \bar{u}_{j,j} - \bar{\rho}_{,j} \bar{u}_{j} T' + \bar{\rho} \bar{T} u'_{j,j}] + \frac{\gamma}{\Pr \text{Re}} [\bar{\kappa} T'_{,i} + \kappa' \bar{T}_{,i}]_{,i} +$$

$$(10)$$

$$\frac{\gamma(\gamma-1)M^2}{\mathrm{Re}}\left[2\bar{\lambda}\,\bar{S}_{ii}S'_{jj}+\lambda'\bar{S}_{ii}\bar{S}_{jj}+4\bar{\mu}\,\bar{S}_{ij}S'_{ij}+2\mu'\bar{S}_{ij}\bar{S}_{ij}\right]$$

$$p' = (\bar{\rho} T' + \bar{T} \rho')/(\gamma M^2) \tag{11}$$

## 2.2 Numerical Method

To ensure the convergence of base flow to steady state, initial conditions are obtained by solving the compressible potential flow equations. On wall and symmetry boundaries, the normal derivative of velocity potential  $\partial \phi/\partial n$  is set to zero, i.e., no-penetration condition. On inflow/outflow boundaries, the velocity potential is set to freestream value.

To obtain base flow, a fourth-order finite-difference scheme is used for spatial discretization. A first-order implicit-Euler time stepping scheme is used to advance the governing equations in time. All boundary conditions are fully implicit to preserve convergence. On the wall, the no-slip velocity boundary conditions are implemented, and the temperature boundary condition is either isothermal condition,  $T = T_w$ , or adiabatic condition  $\frac{\partial T}{\partial n} = 0$ . On the inflow boundary, the boundary conditions are based on the locally one-dimensional Riemann invariants. On the outflow boundary, a parabolic outflow condition is applied to insure the stability and convergence[7].

To solve the linearized disturbance equations, the unsteady equations are advanced in time using the second-order accurate, implicit scheme. Given the base flow solution, the disturbance equations are solved by a combination of fourth-order finite difference and a spectral scheme in the homogeneous direction to accurately calculate the spatial derivative. On the wall, the undisturbed surface boundary conditions are same as the wall boundary conditions used for the base flow. On the inflow/outflow boundaries, non-reflection conditions are applied to ensure the unstable waves not to pass through the computation boundary[7].

#### 2.3 Validation

To study the leading-edge acoustic receptivity, a flat plate with an elliptic leading edge is mostly employed[3]. However, the curvature at the junction between the ellipse and the flat plate is discontinuous, which leads to a source of receptivity. Lin confirmed this computationally[8], and then introduced a new leading-edge geometry based on a modified super-ellipse (MSE) given by

$$[(a-x)/a]^m + [y/b]^n = 1, \quad 0 < x < AR, \quad 0 < y < 1,$$
(12)

where a and b are the semi-major axis of the ellipse and the half-thickness of the plate (the reference length scale), and the aspect ratio AR = a/b.

In this section, AR = 6, m = 4, n = 2, and the geometry of MSE is given in Figure 1(a). By using MSE (same AR as the ordinary ellipse), the curvature discontinuity at junction can be eliminated, as shown in Figure 1(b), which avoids the geometrical uncertainty on the receptivity. In addition, MSE has the further advantage of having a nose curvature (hence a pressure distribution) close to that of an ordinary ellipse.

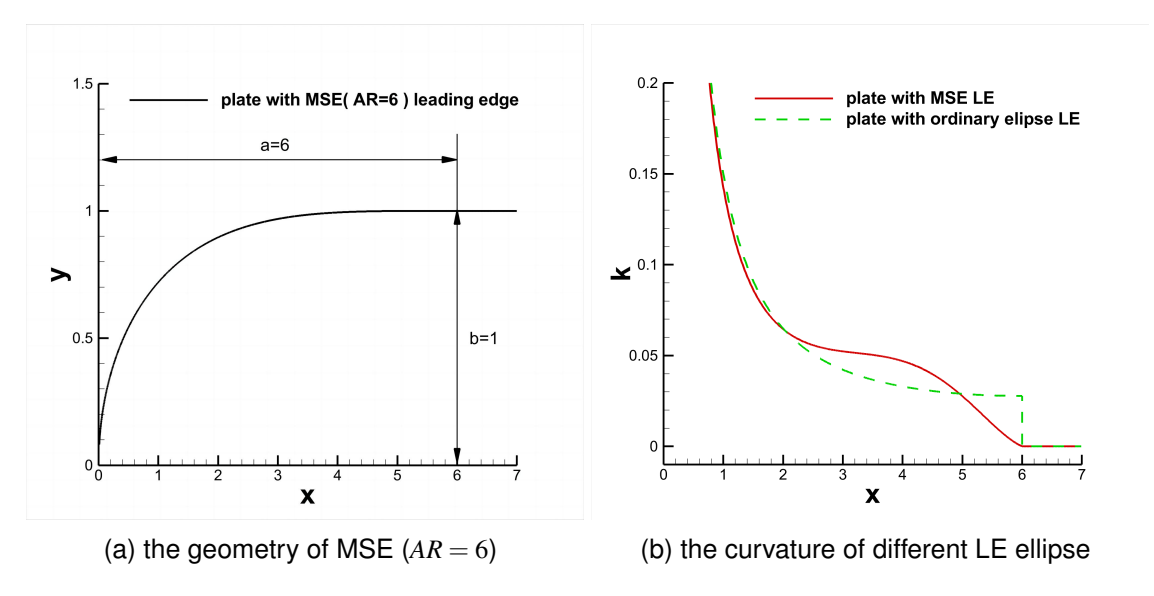


Figure 1 – The geometry and curvature of a plate with MSE leading edge (AR = 6, the junction at x = 6).

The acoustic disturbance excites the receptivity in the boundary layer in the form of pressure fluctuation. The incident plane acoustic wave with a dimensionless wavelength  $\lambda$  is given by

$$p_i = p_0 e^{ik(x-t)}, \quad k = \frac{2\pi}{\lambda} \tag{13}$$

where  $p_0$  is the pressure amplitude, and the direction of sound propagation is the positive x-axis.

To validate the base flow and receptivity, the incompressible study of Collis[7] is used as a validation case. The wall pressure distribution and streamwise velocity profiles of the base flow at Mach number M=0.1 are compared with those of Collis[7] at Reynolds number  $Re=U_{\infty}b/v=2400$ , as shown in Figure 2, where the reference length is the half flat plate thickness b, and the Blasius variable  $\eta_b=y\sqrt{Re/x}$ . It can be seen that the agreement is excellent.

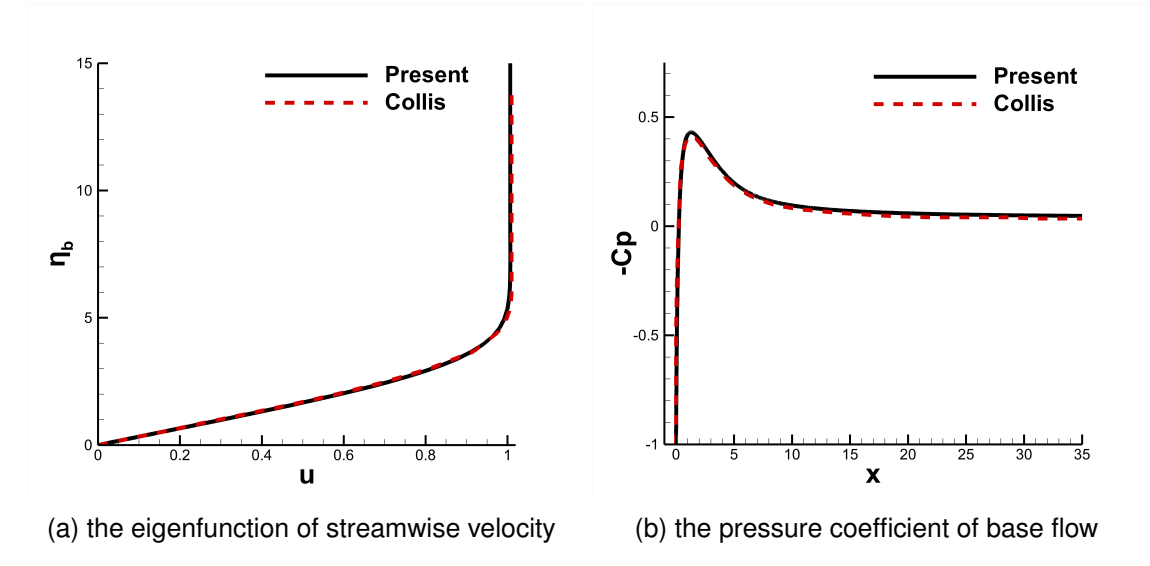


Figure 2 – Comparisons of the pressure coefficient and streamwise velocity of base flow(M = 0.1) with those of Collis[7].

Acoustic plane wave without incidence angle at dimensionless circular frequency  $\omega=0.552$  is enforced at the inlet, corresponding to dimensionless frequency parameter  $F=\omega/Re\times 10^6=230$  where Re=2400. When Mach number M=0.1, this frequency corresponds to the downstream propagating acoustic wave with dimensionless wavelength  $\lambda=125$ . At simulation time t=65.45, corresponding to forced acoustic disturbance period T=11.38, the periodic evolution of T-S waves on the flat plate can be observed from the vertical disturbance velocity distribution, as shown in Figure 3, which is compared with the results of Collis's[7]. By calculating the average distance between a series of T-S wave peaks or troughs, the wavelengths of T-S waves are obtained. It can be seen that there are T-S waves near the wall, and the wavelength  $\lambda=4.32$  is equal to that of Collis's.

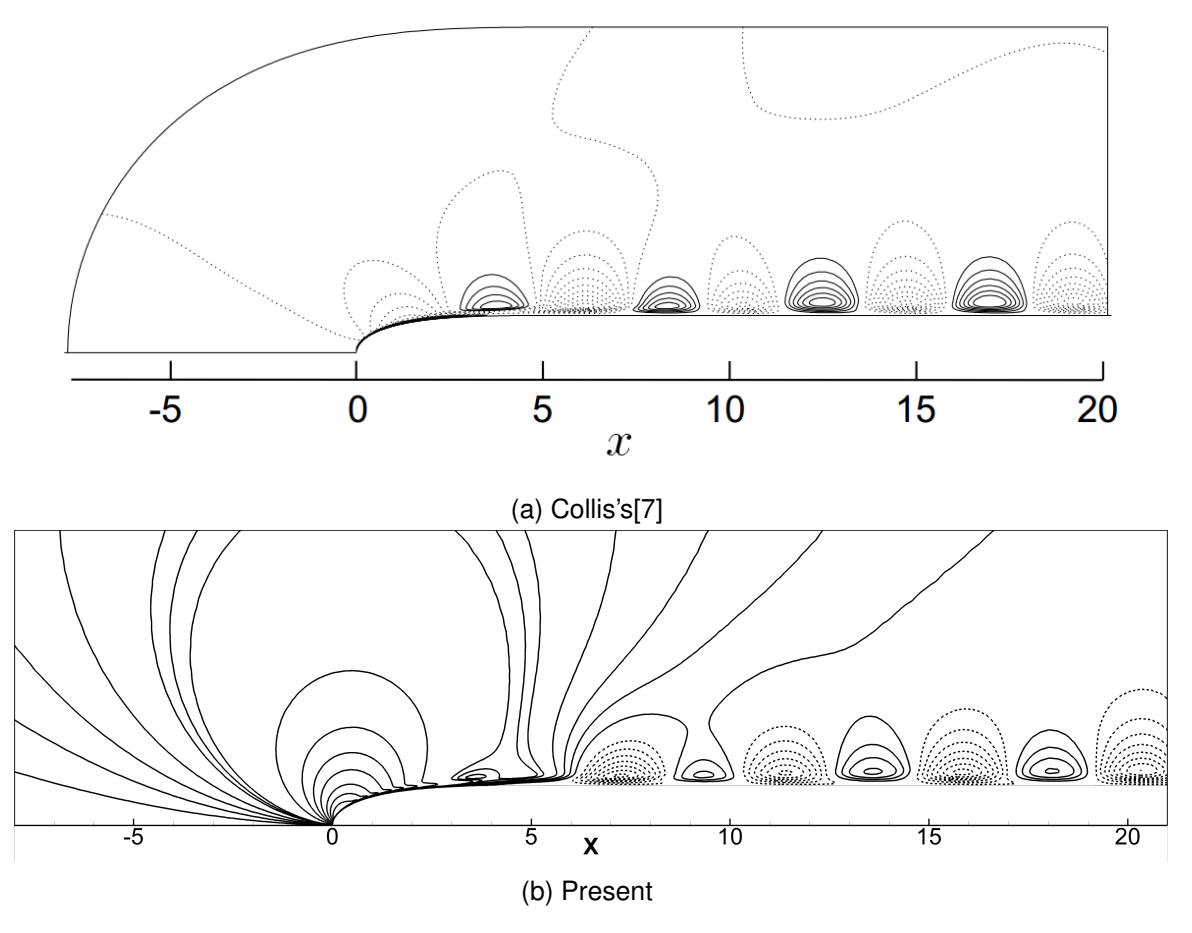


Figure 3 – Comparison of vertical disturbance velocity with that of Collis's Contours from -0.002 to 0.002 with increment 0.0002. Solid lines indicate positive velocity while dotted lines indicate negative velocity.

In both experiments and numerical simulations, extracting T-S waves from the disturbances with the same frequency is very critical. To separate the T-S and the diffracted acoustic components, Murdock suggested that the spatial-average magnitude of disturbances is associated with the diffracted acoustic waves, while the oscillation magnitude around the average is linked to T-S waves[8]. The total disturbance contains both acoustic and T-S components at the same frequency but with different wave velocities, which results in different wavelengths. The disturbance outside the boundary layer at y = 19 solely consists of acoustic component, as shown in Figure 4, while the disturbance in the boundary layer at y = 0.2 comprises both acoustic waves and T-S waves. By subtracting the former from the latter, the streamwise disturbance velocity of T-S waves can be obtained[9]. In fact, it needs to verify whether the extracted wave is T-S wave. Since complex plane decomposition to disturbances is not used here, the disturbance profile is only obtained at the streamwise position where the acoustic disturbance component is small. The extracted wave at  $R = \sqrt{Re_x} = 260$  is, compared with Linear Stability Theory (LST) simulation at same R, as shown in Figure 5. The T-S wave has a peak quite near the wall, then undergoes phase transformation, and finally gradually decays away from the wall, which is consistent with the evolution of T-S wave in the boundary layer[10]. But due to the slight pressure gradient, i.e, the non-parallel effect, the disturbance profile of T-S wave has some differences gradually away from the wall.

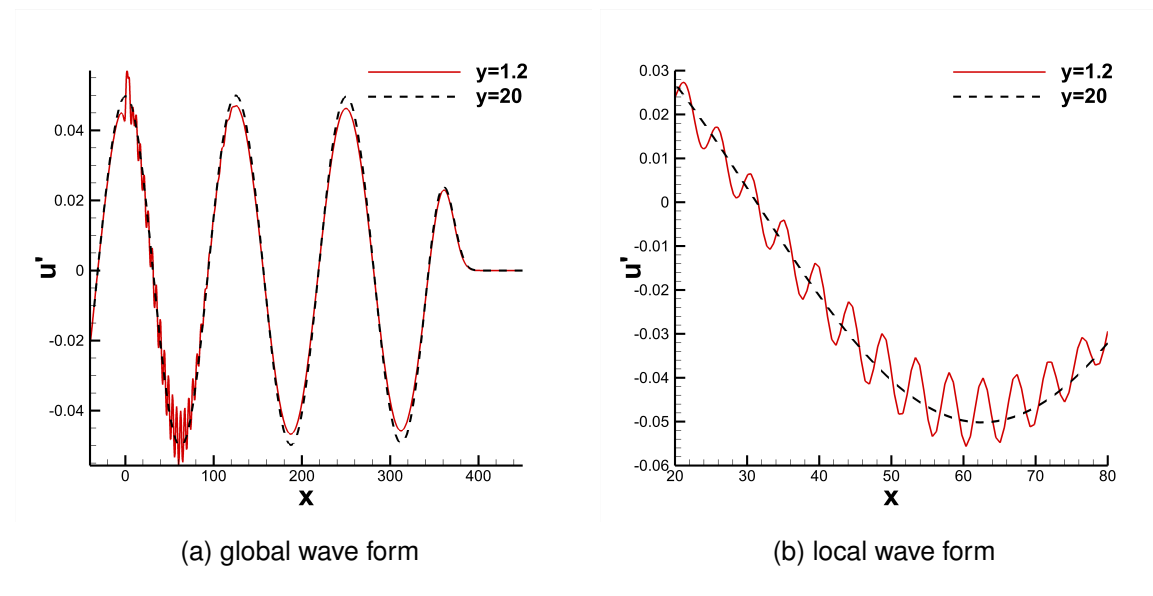


Figure 4 – Streamwise disturbance velocity at different wall-normal distances.

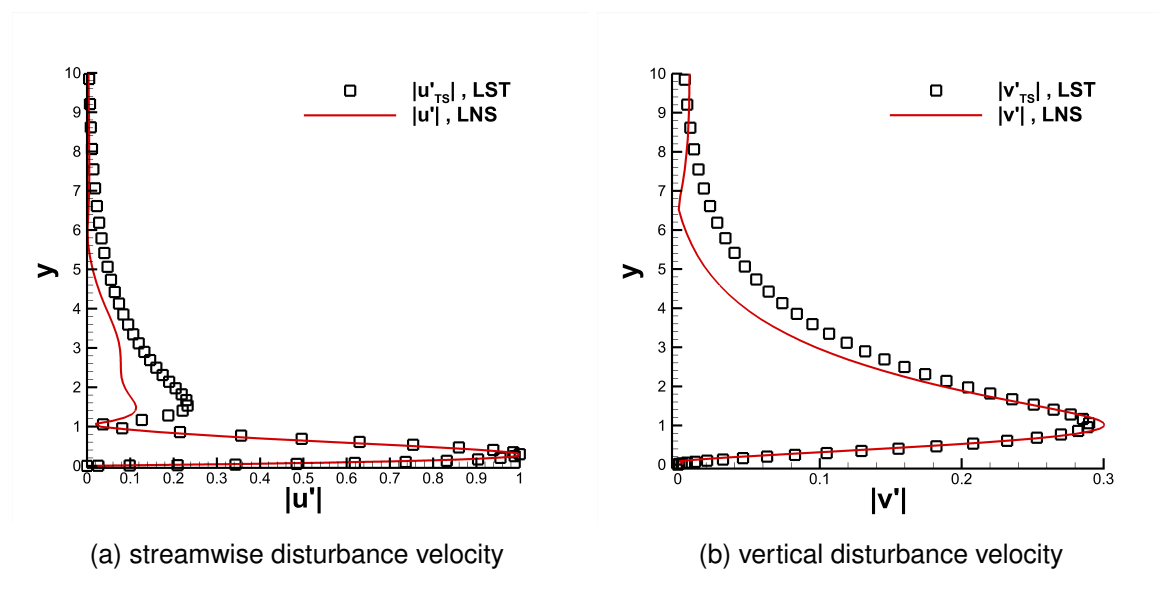


Figure 5 – Disturbance velocity profile at  $R = \sqrt{Re_x} = 260$  compared with those of LST.

## 3. Acoustic Receptivity Study

# 3.1 Incompressible Acoustic Receptivity simulation (M = 0.1)

It can be seen that the acoustic receptivity computation at M=0.1 is a good approximation of that of incompressible flow. Comparing T-S wavelengths with the corresponding acoustic wavelengths of other four cases, as given in Table 1, which confirms the wavelength transformation mechanism of the subsonic boundary layer's receptivity. It also shows that the T-S wavelength  $\lambda_{TS}$  increases with the decrease of the nondimensional frequency parameter F, and independent of the variation of aspect-ratio AR.

Theoretically, the wall-normal disturbance velocity of Stokes waves is small compared to T-S waves of the same frequency in the boundary layer, indicating that the wall-normal perturbation velocity is the main response to T-S waves. It is possible to observe how the wall-normal disturbance velocity at a certain wall distance varies with the Reynolds number (streamwise position). By determining the location where the disturbance velocity  $v'_{TS}$  begins to grow, an estimate of Branch-I location  $R_1$  can be obtained. Based on the location where the streamwise perturbation velocity  $u'_{TS}$  begins to grow, an estimate of Branch-I location  $R_2$  can be obtained. Compare estimations with theoretical neutral-stability curve of incompressible (M = 0.1) flat plate[11], the estimated  $R_2$  is closer to the theoretical

Table 1 – Comparison between wavelengths of T-S waves and acoustic waves.

case	М	Re	$F \times 10^6$	AR	$\lambda_{ac}$	$\lambda_{TS}$
а	0.1	2400	90	6	319.9	9.82
b	0.1	2400	90	20	319.9	10.02
С	0.1	2400	60	6	480	13.84
d	0.1	2400	120	6	240	7.68
е	0.1	2400	230	6	125.2	4.54

value  $R_0$ , as shown in Figure 6(a), thus  $R_2$  is selected as Branch-I location in the following section. The receptivity coefficient  $K_I = |u'_{TS}|/|u'_{ac}|$  at  $R_2$ , where  $u'_{ac}$  is freestream acoustic disturbance magnitude, is compared with the incompressible numerical simulation results of Shahriari et al.[12]. The trend is quiet consistent, as shown in Figure 6(b).

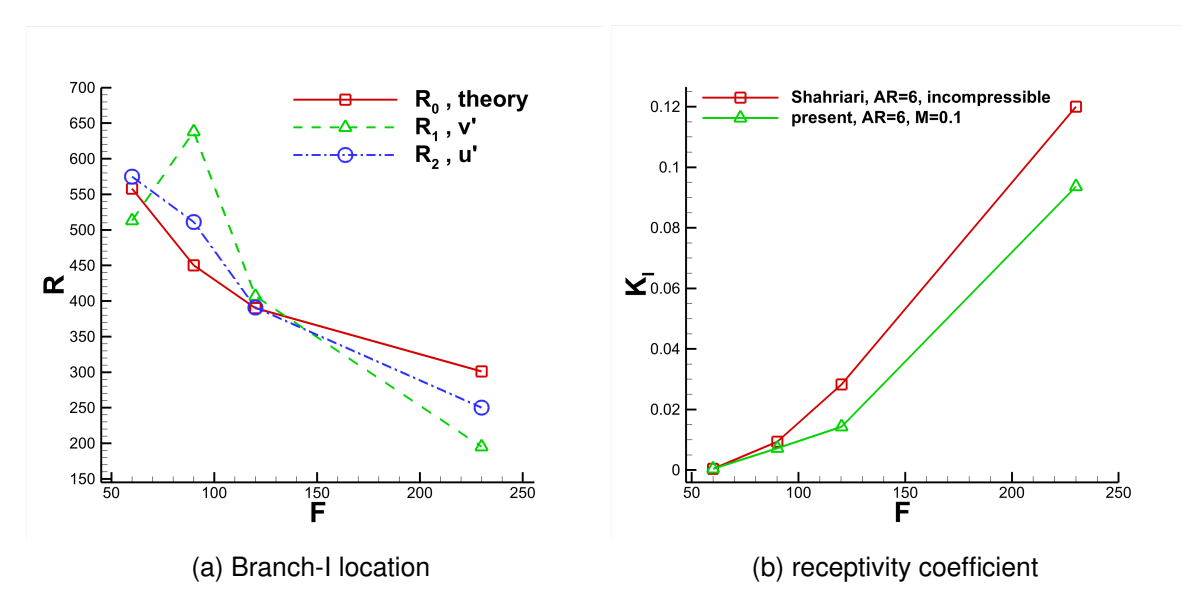


Figure 6 – Comparison of the effect of disturbance frequency on receptivity and stability.

## 3.2 Compressible Acoustic Receptivity (M = 0.4, 0.6)

To study the effects of disturbance frequency F, MSE leading-edge aspect-ratio AR, and Mach number M on the leading-edge acoustic receptivity, four compressible cases with different parameters are simulated, as listed in Table 2. The Branch-I location  $R_2$  goes upstream when F and M increase, as shown in Figure 7(a). However, the effect of AR is quite weak. The receptivity coefficient  $K_I$  increases, when AR decreases or F increases, as shown in Figure 7(b), but the effect of M is not obvious. The amplitudes of T-S wave streamwise disturbance velocity  $u_{TS}$  and vertical disturbance velocity  $v_{TS}$  increase when F increases or M increases, as shown in Figure 8.

Table 2 – Parameter of different cases.

case	M	Re	$F \times 10^6$	AR
f	f 0.4		90	6
g	0.4	2400	230	6
h	0.6	2400	90	6
i	0.6	2400	230	6

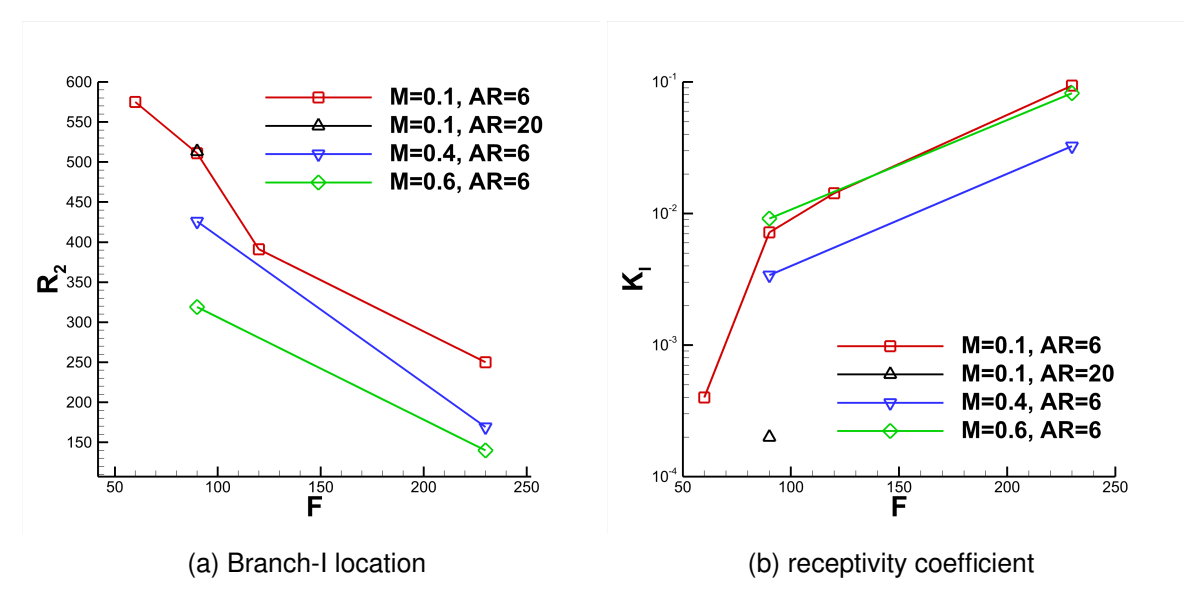


Figure 7 – The effects of disturbance frequency, aspect ratio, Mach number on receptivity and stability.

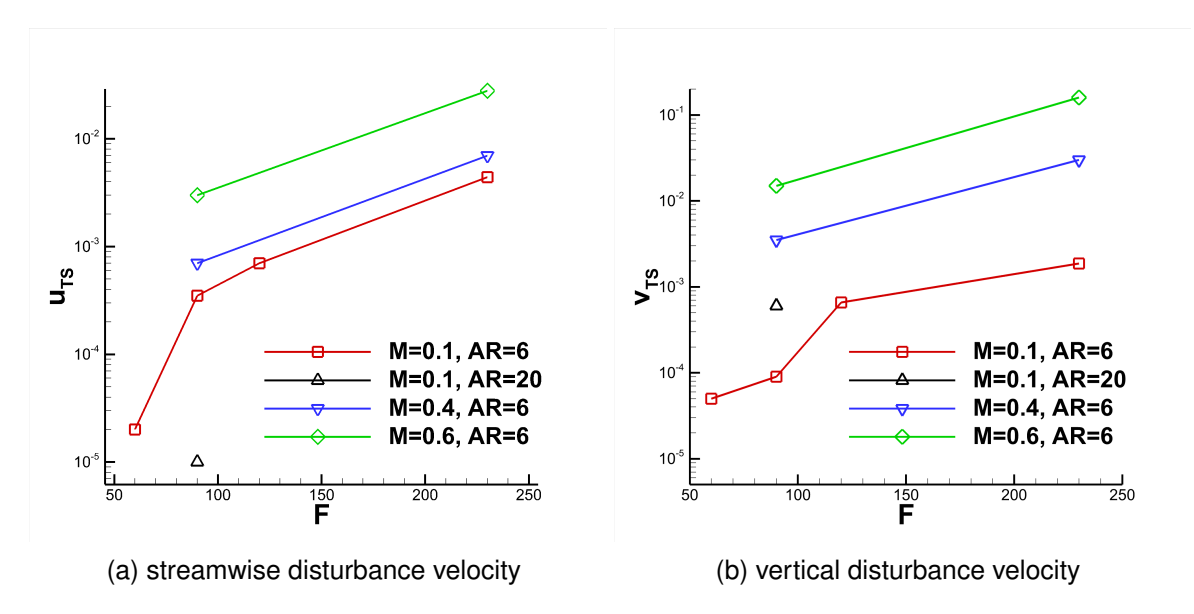


Figure 8 – The effects of disturbance frequency, aspect-ratio, Mach number on T-S wave disturbance velocity.

Mach number M and disturbance frequency F have significant impact on the T-S wave eigenfunctions, as shown in Figure 9(a) and (b) for streamwise and wall-normal disturbance velocity, respectively. However, the leading-edge aspect-ratio AR has weak effect on the disturbance velocity profiles. Density and temperature disturbances in the boundary layer can be observed exhibiting distribution similar to that of the streamwise disturbance velocity, as shown in Figure 9(c) and (d). It can be seen that AR has small impact on the density and temperature disturbance profiles, but M has a strong effect.

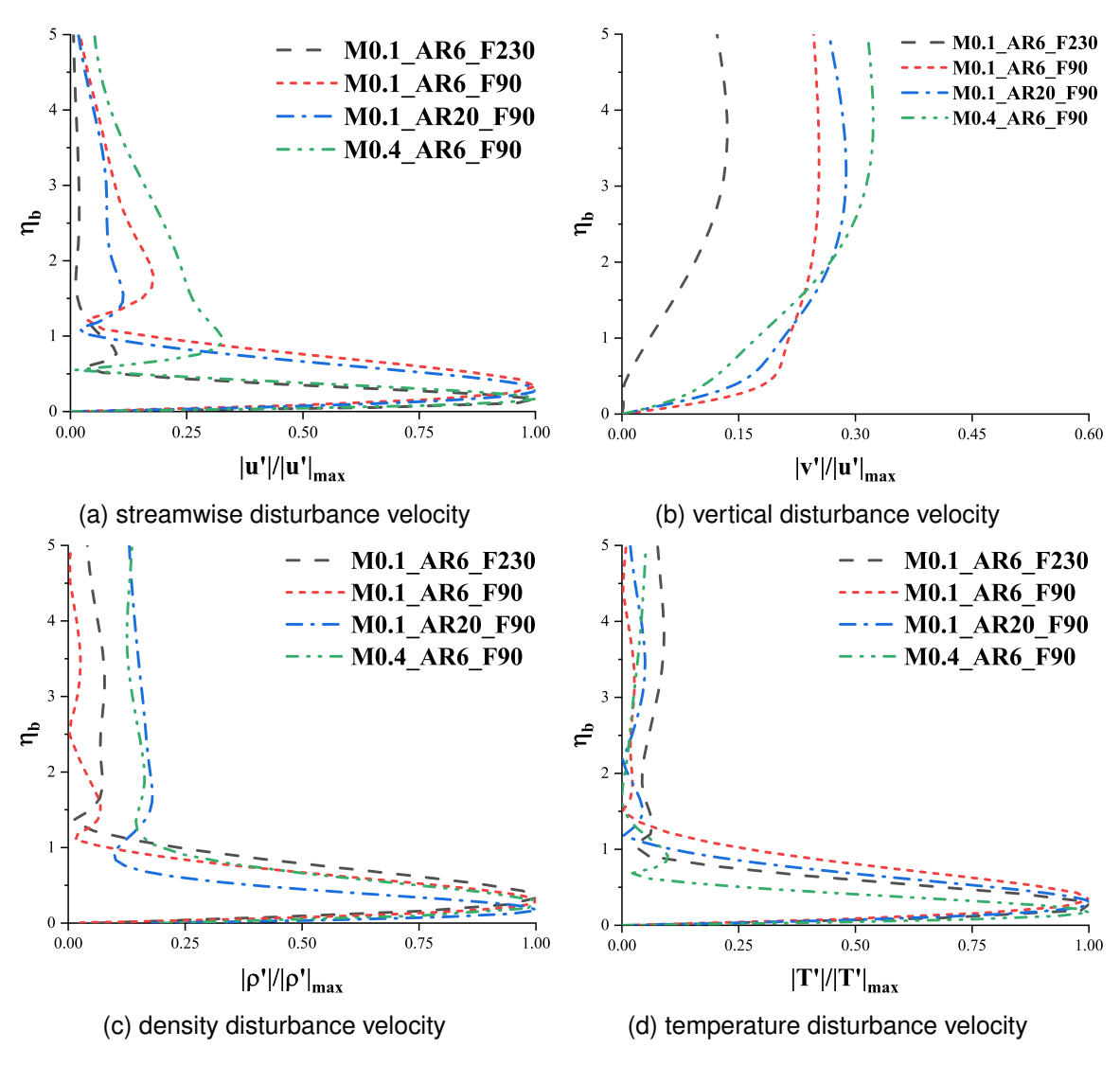


Figure 9 – Comparisons of T-S wave profiles at  $R = \sqrt{Re_x} \approx 400$  with different frequency, aspect-ratio, Mach number.

In the range of M and AR studied in this work, AR has greater impact on receptivity coefficient. The distributions of wall-pressure coefficient and wall-pressure gradient for the four cases are shown in Figure 10. When the leading edge is blunt with AR = 6, the pressure distributions have low pressure peaks near the leading edge and a strong favorable pressure gradient followed by a strong adverse pressure gradient. However, for the leading edge with AR = 20, the pressure peak and the corresponding gradient are both quite weak, which may be used to interpret the very lower receptivity coefficient, as shown in Figure 7(b).

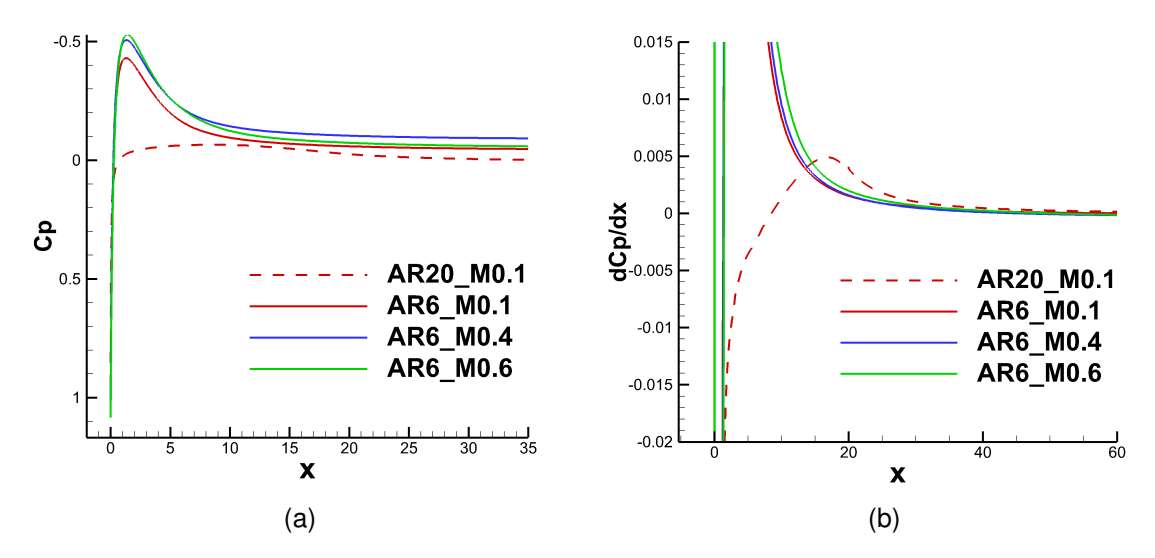


Figure 10 – Comparisons of wall-pressure coefficient and wall-pressure gradient).

#### 4. Confusions

The effect of receptivity on stability and flow transition prediction is critical and the effects of flow parameters, external disturbances, object geometry and surface distribution on receptivity processes still need to be further studied. In present work, the numerical simulations are used to study the acoustic receptivity of compressible laminar flow over a flat plate with modified super-ellipse leading edge, the following conclusions can be drawn:

- (1)The transformation of the long-wavelength acoustic disturbance to the short-wavelength T-S wave is observed, and the wavelength conversion mechanism of the subsonic boundary layer receptivity is confirmed.
- (2)Acoustic disturbance frequency F, modified super-ellipse aspect ratio AR and Mach number M all have important effects on the leading-edge acoustic receptivity, the receptivity coefficient  $K_I$  increases with increasing M, decreasing AR or increasing F. Acoustic disturbance frequency F and Mach number M have important effects on the Branch-I location. Branch-I location moves upstream when increasing M or F, but AR has little effect.
- (3)Local pressure gradient near the leading edge, i.e., local base flow change near the leading edge in a small streamwise scale, has an important impact on the acoustic receptivity. The locations of pressure-gradient peak and onset of zero-pressure gradient move downstream with increasing leading-edge aspect ratio AR, but the sub-critical Mach number M has very weak effect.

## 5. Acknowledgement

# 6. Contact Author Email Address

zhenlichen@nwpu.edu.cn

## 7. Copyright Statement

The authors confirm that they, and/or their company or organization, hold copyright on all of the original material included in this paper. The authors also confirm that they have obtained permission, from the copyright holder of any third party material included in this paper, to publish it as part of their paper. The authors confirm that they give permission, or have obtained permission from the copyright holder of this paper, for the publication and distribution of this paper as part of the ICAS proceedings or as individual off-prints from the proceedings.

#### References

- [1] Morkovin M V. On the many faces of transition. *Viscous Drag Reduction*: Proceedings of the Symposium on Viscous Drag Reduction held at the LTV Research Center, Dallas, Texas, September 24 and 25, 1968. Springer US, 1969: 1-31.
- [2] Schmid P J, Henningson D S. Stability and transition in shear flows. New York: Springer-Verlag, 2001.
- [3] Saric W S, Reed H L, Kerschen E J. Boundary-layer receptivity to freestream disturbances. *Annual review of fluid mechanics*, 2002, 34(1): 291-319.
- [4] Goldstein M E. The evolution of Tollmien–Schlichting waves near a leading edge. *Journal of Fluid Mechanics*, 1983, 127: 59-81.
- [5] Goldstein M E. Scattering of acoustic waves into Tollmien-Schlichting waves by small streamwise variations in surface geometry. *Journal of Fluid Mechanics*, 1985, 154: 509-529.
- [6] Haddad O M, Corke T C. Boundary layer receptivity to free-stream sound on parabolic bodies. *Journal of Fluid Mechanics*, 1998, 368: 1-26.
- [7] Collis S S. A computational investigation of receptivity in high-speed flow near a swept leading-edge. Stanford university, 1997.
- [8] Lin N, Reed H L, Saric W S. Effect of leading-edge geometry on boundary-layer receptivity to freestream sound. *Instability, Transition, and Turbulence*. Springer New York, 1992: 421-440.
- [9] Murdock J W. The generation of a Tollmien-Schlichting wave by a sound wave. *Proceedings of the Royal Society of London. A. Mathematical and Physical Sciences*, 1980, 372(1751): 517-534.
- [10] Mack L M. Linear stability theory and the problem of supersonic boundary-layer transition. *AIAA journal*, 1975, 13(3): 278-289.
- [11] Masad J A, Abid R. On transition in supersonic and hypersonic boundary layers. *International journal of engineering science*, 1995, 33(13): 1893-1919.
- [12] Shahriari N, Bodony D J, Hanifi A, et al. Acoustic receptivity simulations of flow past a flat plate with elliptic leading edge. *Journal of Fluid Mechanics*, 2016, 800: R2.
- [13] Mack L M. Boundary-layer linear stability theory. California Inst of Tech Pasadena Jet Propulsion Lab, 1984.
- [14] Schlichting H, Gersten K. Boundary-layer theory. Springer, 2016.
- [15] Reed H L, Saric W S, Arnal D. Linear stability theory applied to boundary layers. *Annual review of fluid mechanics*, 1996, 28(1): 389-428.
- [16] Hammerton P W, Kerschen E J. Boundary-layer receptivity for a parabolic leading edge. *Journal of Fluid Mechanics*, 1996, 310: 243-267.
- [17] Hammerton P W, Kerschen E J. Effect of leading-edge geometry and aerodynamic loading on receptivity to acoustic disturbances. *Laminar-Turbulent Transition*: IUTAM Symposium, Sedona/AZ September 13–17, 1999. Springer Berlin Heidelberg, 2000: 37-42.